

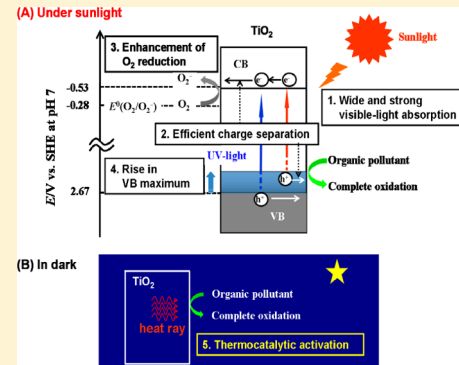
Molecular-Scale Transition Metal Oxide Nanocluster Surface-Modified Titanium Dioxide as Solar-Activated Environmental Catalysts

Hiroaki Tada,*[†] Qiliang Jin,[†] Anna Iwaszuk,[‡] and Michael Nolan*,[‡]

[†]Department of Applied Chemistry, School of Science and Engineering, Kinki University, 3-4-1, Kowakae, Higashi-Osaka, Osaka 577-8502, Japan

[‡]Tyndall National Institute, University College Cork, Lee Maltings, Prospect Row, Cork, Ireland

ABSTRACT: The development of environmental catalysts is an urgent subject to be tackled by scientists and engineers all over the world due to the borderless nature of environmental pollution. We named the catalyst enabling the decomposition of the pollutants by effectively utilizing the solar energy from ultraviolet to infrared as “solar environmental catalysts”. This Feature Article reviews the recent studies on a novel class of solar environmental catalysts consisting of TiO₂ and molecular scale oxides of 3d metals and for comparison d¹⁰ (Sn) on the surface (MOs/TiO₂). The TiO₂ surface modification with MO clusters by the chemisorption–calcination cycle (CCC) technique presents novel band engineering for finely tuning the top of the valence band, while the unique physicochemical and electronic properties of MOs/TiO₂ give rise to the outstanding photo- and thermocatalytic activities for the decomposition of organic pollutants. In the first part following the Introduction, the CCC technique for forming extremely small MO clusters on TiO₂, the structures, physicochemical properties, and electronic structures of MOs/TiO₂ are described. The second part deals with their thermo- and photocatalytic activities for the degradation of model organic pollutants and the essential action mechanisms of the MO clusters. The combination of experiments and first-principles density functional theory simulations shows that Co₂O₃/TiO₂ can be a prototype of the solar environmental catalyst with high levels of photo(UV and visible)- and thermocatalytic activities.



1. INTRODUCTION

TiO₂-based photocatalysts possess great potential as environmental catalysts for decomposing pollutants in ambient water and air owing to their strong oxidation ability, high physicochemical stability, abundance in nature, and non-toxicity.^{1,2} However, unmodified TiO₂ with a band gap larger than 3 eV only absorbs UV light ($\lambda < 400$ nm) occupying ~3% of the solar energy incident on the earth. Strong absorption in a wide wavelength range of visible light (400 nm $< \lambda <$ 750 nm) with ~45% in the energy maximizes use of the available solar energy and is thus a prerequisite for the effective use of the sunlight (first requirement, Scheme 1). For this purpose, doping of various transition metal cations and nonmetal anions into TiO₂ has been extensively studied.^{3–5} However, in most cases, the emergence of the visible-light response can sacrifice the UV-light activity of TiO₂, which is still important in many applications to increase the overall photocatalytic activity. This arises since doping TiO₂ with a metal cation generates impurity and/or vacancy levels in the bulk that act as recombination centers. Consequently, effective charge separation is of primary importance for achieving the compatibility of high levels of visible- and UV-light activities of TiO₂ (second requirement). In the TiO₂-photocatalyzed decomposition of organic pollutants, the conduction band (CB) electrons reduce O₂, while the valence band (VB) holes oxidize the organic

pollutants directly and/or indirectly.⁶ The driving force for one-electron reduction of O₂ (standard redox potential $E^0(O_2/O_2^-)$ = -0.28 V vs standard hydrogen electrode, SHE) by the excited electrons in the CB (-0.53 V at pH 7) is small. Accordingly, enhancing the O₂ reduction reaction is also necessary for boosting the photocatalytic activity of TiO₂ (third requirement). TiO₂ is usually studied in one of the two crystal forms of anatase and rutile or composites of rutile and anatase.⁵ For decomposition of organic compounds, anatase generally exhibits higher UV-light activity than rutile.^{7,8} Also, the photocatalytic activity can be further increased by coupling anatase and rutile.⁹ The higher activity of anatase with CB edge ~0.2 eV higher than that of rutile also points to the importance of the O₂ reduction. Therefore, in the design for the TiO₂-based visible-light photocatalysts, the VB maximum should be raised without modifying the position of its CB minimum (fourth requirement).

It is worth noting that the infrared ray ($\lambda > 750$ nm) occupies as much as ~52% of the solar energy. However, if charge carriers are generated in photocatalysts by infrared ray irradiation, they could not decompose organic pollutants

Received: December 16, 2013

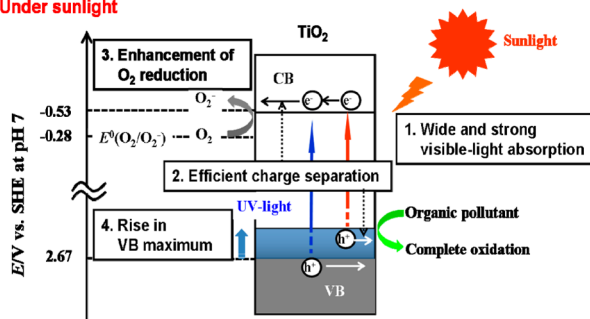
Revised: February 28, 2014

Published: April 4, 2014



Scheme 1. Requirements for the TiO₂-Based Solar Environmental Catalyst

(A) Under sunlight



(B) In dark



because of the small redox ability. The most serious drawback shared by photocatalysts is that they do not work in the dark, i.e., thermally, which significantly narrows their applications. Thus, an ideal environmental catalyst should have high levels of photo(visible and UV light)- and thermocatalytic activities for the degradation of environmental pollutants (fifth requirement).

Kisch and co-workers first devised the photosensitization of TiO₂ with the grafting of metal halides such as PtCl₆²⁻ by using the impregnation method.¹⁰ This approach is attractive in that visible-light response can be induced by the simple procedure without introduction of the impurity/vacancy levels. The research groups of Hashimoto and Ohno have developed the procedure for grafting 3d metal ions such as Cr³⁺,¹¹ Cu²⁺,¹² and Fe³⁺,^{13,14} on TiO₂. The grafting of 3d metal ions on rutile TiO₂ gives rise to a high level of visible-light activity; unfortunately, the effect is much smaller for anatase TiO₂.¹⁴

On the other hand, we have developed the chemisorption–calcination cycle (CCC) technique, where metal complexes are adsorbed via chemical bonds and the organic part is oxidized by postheating, for preparing extremely small clusters and ultrathin films of MOs.¹⁵ This approach, in collaboration with first-principles density functional theory (DFT) simulations, provides a novel approach to modify TiO₂ (anatase and anatase–rutile) for a high level of visible and UV photocatalytic activity for degradation of organic molecules. This Feature Article summarizes our recent experimental and DFT studies on molecular 3d MOs/TiO₂, and the results are compared with those for the d¹⁰ MO (SnO₂)-surface modified TiO₂.

2. CATALYST PREPARATION

Two kinds of TiO₂ particles (ST-01 (anatase), specific surface area = 309 m² g⁻¹, Ishihara Sangyo and P-25 (anatase/rutile = 4/1 w/w), specific surface area = 50 m² g⁻¹, Degussa) having the highest level of photocatalytic activities among the commercial ones were used. Metal acetylacetones can be strongly adsorbed on the surfaces of TiO₂, and the adsorption mechanism is different for the kinds of metal complexes. Fe(acac)₃ is chemisorbed on TiO₂ via the ligand exchange between the acac ligand and the surface Ti–OH group.¹⁶ Also, Cu(acac)₂ adsorbed on TiO₂ proceeds via the surface coordination of the Ti_s–OH group without elimination of

the acac ligands.¹⁷ On the other hand, the adsorption of [Sn(acac)₂]Cl₂ on the TiO₂ surface proceeds by way of the ion exchange between H⁺ and the [Sn(acac)₂]²⁺ ion.¹⁸

The impregnation method has conventionally been used for loading MO NPs on the supports. On the other hand, the CCC technique is designed to form not MO NPs but molecular-scale MO clusters on TiO₂ by using metal acetylacetones as a precursor and nonaqueous solvent to restrict the hydrolysis–polymerization. For example, iron oxide clusters can be formed on the TiO₂ surface via the following three steps.¹⁶ At the first step, Fe(acac)₃ is chemisorbed on the TiO₂ surface from a nonaqueous solution. The resulting solids are washed repeatedly with the solvent for the physisorbed complexes to be removed. At the second step, the oxidation of the acac ligands by heating the samples in air at 773 K yields iron oxide clusters on the TiO₂ surface. These procedures are repeated to increase the Fe loading amount. Chemical analysis confirmed that all the Fe is present only on the TiO₂ surface. The Fe loading amount is expressed by the number of Fe ions per unit TiO₂ surface area ($\Gamma/\text{ions nm}^{-2}$). By using the CCC technique, the MO loading amount can be precisely controlled in a wide range by the complex concentration and cycle number. This is a feature of the CCC technique, which is conveniently applicable for the formation of other MO clusters on both TiO₂ particles¹⁶ and films.¹⁹

3. STRUCTURES

3.1. Experiment. A key feature of the CCC technique is the formation of extremely small MO clusters on the TiO₂ surface in a high dispersion state. No particles were observed on the TiO₂ surface at $\Gamma \leq 0.54$ for iron oxide/TiO₂¹⁶ and at $\Gamma \leq 0.15$ for cobalt oxide/TiO₂ by transmission electron microscopy.²⁰ In the latter, cobalt oxide clusters (<~2 nm) were present on the TiO₂ surface at $\Gamma \geq 0.23$. Molecular-scale MO clusters are deposited on the TiO₂ surface in a highly dispersed state at small Γ region by the CCC technique. To obtain the structural information, Fe K-edge X-ray absorption near-edge structure spectra for the iron oxide/TiO₂ samples and authentic Fe, Fe₃O₄, and α -Fe₂O₃ were measured.¹⁶ The comparison of the absorption edge confirmed that the iron oxidation state in the clusters is 3+. The oxidation states of metal ions in the other MO clusters were determined by X-ray photoelectron spectroscopy (XPS). The iron oxide and cobalt oxide clusters are formally represented by Fe₂O₃ and Co₂O₃, respectively, below. In the Fourier transforms of the k^3 -weighted X-ray absorption fine structure, the Fe–O scattering peak is observed around 1.65 Å, which is significantly shorter than the Fe–O bond length for iron(III) oxides with octahedral coordination (1.91 Å). Whereas the peak assigned to the closest Fe–Fe shell is observed at 2.72 Å for the samples with $\Gamma \geq 0.86$, the peak intensity is very weak at $\Gamma \leq 0.5$. These findings suggest that most Fe(III) oxide species with coordination number smaller than 6 exist as mononuclear clusters on the TiO₂ surface in a high dispersion state at $\Gamma \leq 0.5$.

3.2. DFT Simulation. The relaxed atomic structure of (FeO)₂ and Fe₂O₃ nanoclusters adsorbed at the rutile (110) surface and the computed adsorption energies, denoted E^{ads} , are shown in Figure 1. While the adsorption energies are computed as 0 K energy differences, they do serve to give an indication of the relative stability of adsorbed nanoclusters.^{21–23} The negative adsorption energies signify that the iron oxide species are stable when adsorbed at the TiO₂ surface, and the magnitude of the adsorption energy means that these species

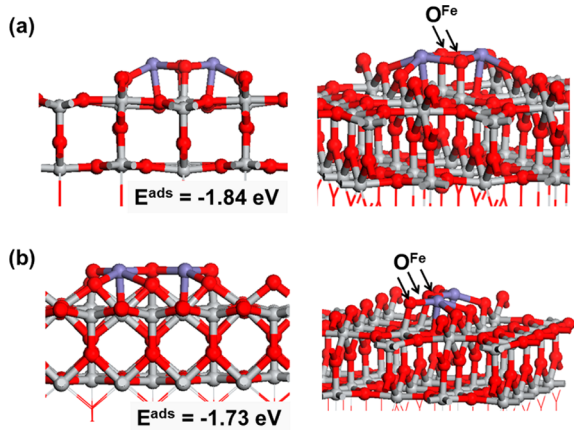


Figure 1. Atomic structure of FeO_x adsorbed at the rutile TiO_2 (110) surface: (a) $(\text{FeO})_2$ and (b) Fe_2O_3 . In this figure, Ti is the gray sphere; O is the red sphere; and Fe is the blue sphere. The adsorption energies, in eV, are shown with each structure, and the oxygen atoms in the iron oxide nanoclusters are indicated by O^{Fe} .

should be thermally stable. Comparing computed entropies of FeO_x nanoclusters to the adsorption energies,²² iron oxide adsorption at the TiO_2 (110) surface is thermodynamically favored. This result holds in general for metal oxide nanoclusters adsorbed at TiO_2 surfaces, which is consistent with their stability in the experiments. In the most stable adsorption structure of Fe_2O_3 , the O and Fe from iron oxide are arranged in a zigzag O–Fe–O–Fe–O, typical of the most stable gas-phase Fe_2O_3 cluster. Each O bonds to a 5-fold coordinated Ti along one row in the TiO_2 surface. The Fe–O distances in adsorbed Fe_2O_3 are 1.82 and 1.93 Å. The Fe–O distances to oxygen in TiO_2 are in the range 2.02–2.09 Å. Finally, the Ti–O distances involving oxygen from Fe_2O_3 are in the range 2.1–2.2 Å. $(\text{FeO})_2$ has a similar adsorption energy to Fe_2O_3 . In this species, each Fe is bound to two bridging oxygen atoms of TiO_2 , with Fe–O distances of 2.11 and 2.29 Å. Oxygen from $(\text{FeO})_2$ binds to a 5-fold coordinated Ti atom from the surface, with Ti–O distances of 1.89 Å. Fe–O distances in $(\text{FeO})_2$ are 2.04/2.12 Å.

Figure 2 shows the atomic structure of Co_2O_3 and Co_4O_6 nanoclusters adsorbed at the rutile (110) surface and Co_4O_6

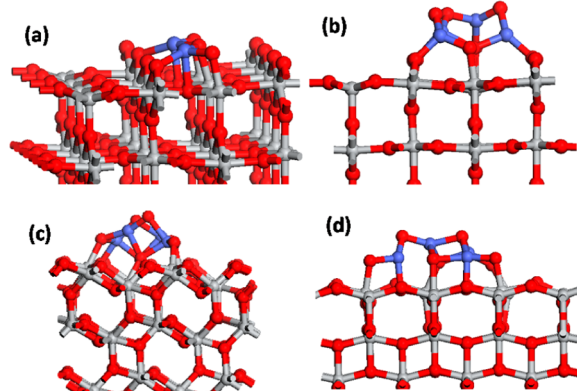


Figure 2. Adsorption structures of CoO_x nanoclusters on TiO_2 surfaces: (a) Co_2O_3 on rutile (110), (b) Co_4O_6 on rutile (110), (c), Co_4O_6 on anatase (101), and (d) Co_4O_6 on anatase (001). In this figure, Ti is gray, O is red, and Co is blue.

adsorbed at the anatase (101) and (001) surfaces. For adsorption of Co_2O_3 and Co_4O_6 nanoclusters on rutile (110), we compute adsorption energies of -5.86 and -5.79 eV, respectively. For adsorption of the Co_4O_6 nanocluster on anatase (101), the computed adsorption energy is -7.31 eV, and at anatase (001), the adsorption energy is -3 eV. Thus, in terms of adsorption, Co_2O_3 nanoclusters will adsorb strongly to TiO_2 surfaces, irrespective of the crystal form of TiO_2 considered. On rutile (110), Co_2O_3 binds in a similar fashion to Fe_2O_3 , with new bonds between Co and oxygen in the nanocluster to the surface. Co–O distances to the rutile surface are 2.05–2.10 Å. Within the nanocluster, the Co–O distances are 1.75 and 1.91 Å, with the shorter distances to the 2-coordinated nanocluster oxygen atoms that bind to the surface. The Co_4O_6 nanocluster binds to the rutile (110) surface with Co–O distances of 1.85–1.98 Å. The Co atoms in this nanocluster have lower coordination to the support surface than in the smaller Co_2O_3 nanocluster. Co–O distances in the nanocluster range from 1.70 to 1.94 Å, with lower coordinated oxygen atoms showing shorter Co–O distances. On the anatase (101) surface, Co–O distances to the surface are 1.84–1.98 Å, while on anatase (001), the Co–O distances are 1.90 Å. Within the Co_4O_6 nanoclusters, the Co–O distances are similar to those for Co_4O_6 supported on rutile, namely, lying in the range 1.74–1.91 Å, with the effect of coordination number again determining the length of the Co–O distances. All supported nanoclusters display low coordinated oxygen species, primarily 2-fold coordinated oxygen species, while Co shows 3- and 4-coordination.

4. PHYSICOCHEMICAL PROPERTIES

4.1. Optical Property. The optical property is of fundamental importance in connection with the photocatalytic activity. Figure 3 compares UV–visible absorption spectra of $\text{Fe}_2\text{O}_3/\text{TiO}_2$ (A), $\text{Co}_2\text{O}_3/\text{TiO}_2$ (B), and $\text{SnO}_2/\text{TiO}_2$ (C), prepared by the CCC technique. While TiO_2 has no absorption in the visible region, $\text{Fe}_2\text{O}_3(\Gamma = 5.5)/\text{TiO}_2$ has a broad absorption band due to the d–d transition around 500 nm in a manner similar to bulk iron oxides (Figure 3A). The Fe^{3+} ion-

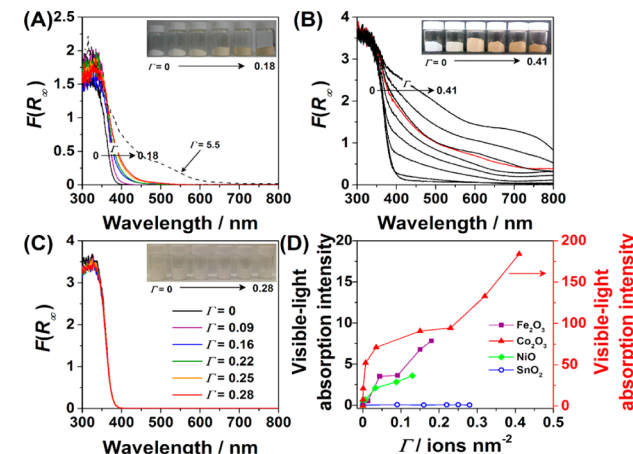


Figure 3. UV–vis absorption spectra of $\text{Fe}_2\text{O}_3/\text{TiO}_2$ (ST-01) (A), $\text{Co}_2\text{O}_3/\text{TiO}_2$ (ST-01) (B), and $\text{SnO}_2/\text{TiO}_2$ (P-25) (C) prepared by the CCC technique: $F(R_\infty)$ denotes the Kubelka–Munk function. In spectra B, the spectrum for the sample with $\Gamma = 0.23$ is shown by red in color. (D) Relative visible-light absorption intensity of MOs/ TiO_2 normalized by the absorption intensity of unmodified TiO_2 .

grafted TiO_2 prepared by the impregnation method has absorption at 410 nm in addition to the d-d transition absorption.^{13,14} The former absorption was ascribable to the electronic transition from Fe^{3+} levels to the CB of TiO_2 . In contrast, the absorption spectra of $\text{Fe}_2\text{O}_3(\Gamma \leq 2.1)/\text{TiO}_2$ show significant band gap narrowing from 3.3 to 2.85 eV as the Γ increases, whereas the d-d transition absorption is very weak. A similar spectral feature was observed also for Cr^{3+} -doped TiO_2 prepared by the physical methods such as ion implantation.²⁴ Also, the Co_2O_3 surface modification causes strong absorption in the whole visible region (Figure 3B). Bulk cobalt oxides have absorption due to the d-d transitions around 650 nm for Co^{2+} ions in tetrahedral coordination and around 500 nm for Co^{3+} ions in octahedral coordination.²⁰ Meanwhile, $\text{Co}_2\text{O}_3(\Gamma \leq 0.15)/\text{TiO}_2$ has featureless absorption at $\lambda < 600$ nm, and the d-d transition absorption appears at $\Gamma \geq 0.23$, where Co_2O_3 NPs were formed on TiO_2 . On the other hand, the surface modification by SnO_2 clusters hardly changes the spectrum of TiO_2 (Figure 3C). Clearly, the 3d MOs/ TiO_2 possess visible-light absorption different from that of the bulk MOs, and significant band gap narrowing is caused by the surface modification with Fe_2O_3 and Co_2O_3 clusters. This unique optical property originates from its extremely small size and highly dispersed state on TiO_2 . Figure 3D compares the visible-light absorption intensity of MOs/ TiO_2 integrated in the wavelength range from 400 to 800 nm. At the same Γ , the visible absorption intensity is on the order of $\text{Co}_2\text{O}_3 > \text{Fe}_2\text{O}_3 > \text{NiO} \gg \text{SnO}_2 \approx \text{unmodified TiO}_2$.

4.2. Band Energy. The VB maximum determining the oxidation ability of the holes is a key factor for the decomposition of organic pollutants by semiconductor photocatalysts. The VB-maximum level of MOs/ TiO_2 can be determined by VB-XPS. Figure 4 shows the VB-XP spectra for $\text{Fe}_2\text{O}_3/\text{TiO}_2$ (A), $\text{Co}_2\text{O}_3/\text{TiO}_2$ (B), and $\text{SnO}_2/\text{TiO}_2$ (C) prepared by the CCC technique. The VB-XP spectra for pristine TiO_2 are shown in Figure 4D. The VB-maximum energy (ΔE_{VBM}) is plotted as a function of Γ in Figure 4D. The ΔE_{VBM} values for Fe_2O_3 , Co_2O_3 , and NiO are positive, indicating that the VB edge of TiO_2 is shifted to higher energy by the presence of these MO clusters. In contrast, the ΔE_{VBM} value for SnO_2 is negative, indicating that the VB edge of TiO_2 is shifted to lower energy by the presence of SnO_2 clusters.

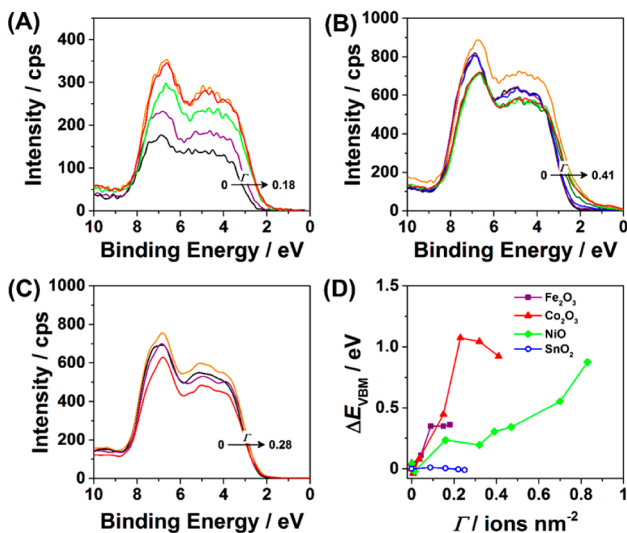


Figure 4. Valence-band XP spectra for $\text{Fe}_2\text{O}_3/\text{TiO}_2$ (ST-01) (A), $\text{Co}_2\text{O}_3/\text{TiO}_2$ (ST-01) (B), and $\text{SnO}_2/\text{TiO}_2$ (P-25) (C) prepared by the CCC technique. (D) VB-maximum for various MOs/ TiO_2 as a function of Γ .

compares the VB-maximum levels for various MOs/ TiO_2 as a function of Γ . The change in the VB-maximum with the surface modification strongly depends on the kind of MO clusters. The rise in the VB-maximum ($\Delta E_{\text{VBM}} = E_{\text{VBM}}(\text{MO}/\text{TiO}_2) - E_{\text{VBM}}(\text{TiO}_2)$) at the same Γ is on the order of $\text{Co}_2\text{O}_3 > \text{Fe}_2\text{O}_3 > \text{NiO} \gg \text{SnO}_2 \approx \text{unmodified TiO}_2$. In the $\text{Co}_2\text{O}_3/\text{TiO}_2$ system, the increment reaches as much as ~ 1 eV at $\Gamma \approx 0.25$. Noticeably, the VB-maximum of TiO_2 can finely be tuned by the loading amount of transition MO clusters. This is the most unique and important feature of the 3d MO cluster surface modification by the CCC technique.

These results were further verified by the DFT simulations. Figure 5 shows the electronic density of states (PEDOS)

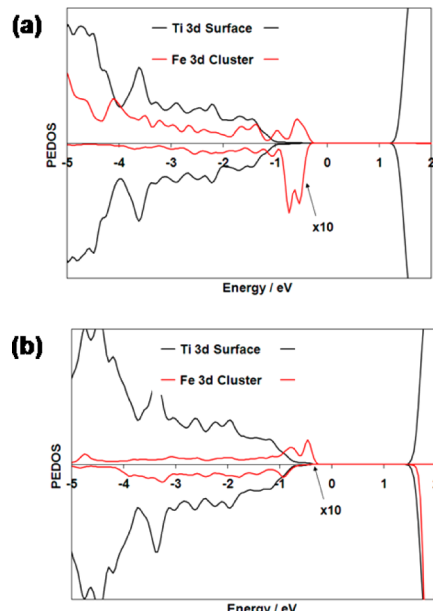


Figure 5. Ti 3d and Fe 3d projected electronic density of states (PEDOS) for FeO_x adsorbed at the rutile TiO_2 (110) surface: (a) FeO and (b) Fe_2O_3 . The PEDOS for Fe in iron oxide is multiplied by 10 to facilitate comparison with the PEDOS from TiO_2 .

projected onto Fe 3d and Ti 3d states for adsorbed $(\text{FeO})_2$ and Fe_2O_3 . The PEDOS plots of FeO_x adsorbed at TiO_2 show that states from adsorbed FeO_x lie above the VB of TiO_2 ; that is, the iron oxide derived states make up the top of the VB in the FeO_x -modified TiO_2 structure. This changes the nature of the VB edge which moves to the top of the VB to higher energy. The offsets between the TiO_2 VB edge and the FeO_x states around the VB are ~ 0.3 eV for both $(\text{FeO})_2$ - and Fe_2O_3 -modified TiO_2 , which is comparable with the experimental value (Figure 4D). For $(\text{FeO})_2$ the Bader charge is +6.52 electrons, and the computed spin magnetization is 4 spins, characteristic of an Fe^{2+} oxidation state. In Fe_2O_3 the Bader charge is +5.5 electrons with computed spin magnetizations of 3 spins on each Fe, typical of an Fe^{3+} oxidation state. All Ti in the surface has computed Bader charges of 1.3 electrons, typical of a Ti^{4+} species, and we have found no Ti^{3+} species. Thus, we find with DFT a change in the energy gap of TiO_2 with iron oxide modification that is independent of the iron oxidation state. In contrast, our recent DFT simulations for the SnO_x ^{23,25} and PbO_x -modified²⁶ TiO_2 systems indicate that the oxidation states ($x = 1$ and 2) have a significant impact on the nature of the modifications of the band edges of TiO_2 or its band gap. In

spite of the intriguing theoretical prediction of the effect of the oxidation state on the band energy, it has not been experimentally confirmed because of the difficulty of the formation of the metal oxide clusters with predetermined oxidation states on TiO_2 .

The PEDOS of Co_2O_3 -nanocluster-modified rutile and anatase TiO_2 (anatase (101) and (001) surfaces) is shown in Figure 6. This system is interesting as it results in the formation

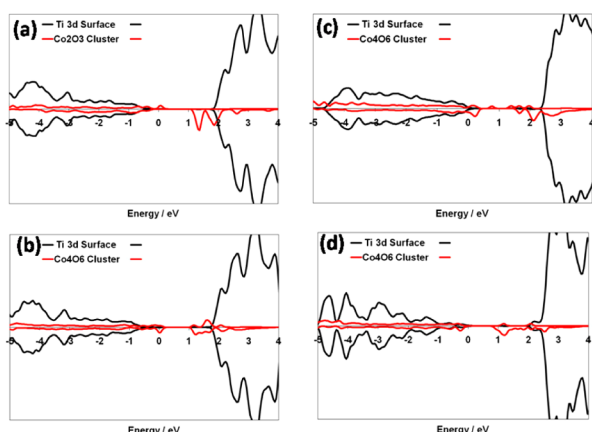


Figure 6. Electronic density of states for Ti 3d and Co 3d states for (a) Co_2O_3 -modified rutile, (b) Co_4O_6 -modified rutile, (c) Co_4O_6 -modified anatase (101), and (d) Co_4O_6 -modified anatase (001).

of new states below the CB edge of the three TiO_2 surfaces considered, irrespective of the crystal form of TiO_2 or the exact surface considered. Here, the Co_2O_3 -derived electronic states appear up to 1 eV below the CB edge of TiO_2 . There are also Co_2O_3 -derived states around the top of the VB edge, which will push the VB edge up in energy, but the modification to the electronic structure by the nanoclusters appears to show some dependence on the nanocluster size and on the exact surface examined. In any case, the energy gap of Co_2O_3 -modified TiO_2 will be strongly reduced over unmodified TiO_2 .

When we compare SnO_2 with other metal oxides such as TiO_2 ^{20,21} or transition metal oxides such as CrO_x and MoO_x ²⁷ or the examples of FeO_x and Co_2O_3 discussed above, the nanocluster-derived electronic states lie above the VB edge of rutile TiO_2 , which pushes the VB edge higher in energy, reducing the VB–CB energy gap over the bare surface. SnO_2 -derived states lie either well separated from the VB and CB edges of TiO_2 for anatase or below the CB edge of TiO_2 (rutile) and will not lead to any significant change in visible-light absorption, which explains the experimental results (see Figure 4C), in which SnO_2 -modified TiO_2 shows no shift to visible-light absorption.

4.3. Oxygen Reduction. In the TiO_2 photocatalytic reaction, the reduction of O_2 by the CB electrons is frequently the rate-determining step.²⁸ Figure 7 shows dark current (I/mA)–potential (E/V vs Ag/AgCl) curves of mesoporous TiO_2 nanocrystalline film-coated FTO (mp- TiO_2 (anatase)/FTO) electrodes without and with MO cluster-surface modification in a 0.1 M NaClO_4 aqueous solution. For the mp- TiO_2 /FTO electrode, only a small current due to the TiO_2 reduction flows at the potential range between 0 and -1 V without O_2 , and the presence of O_2 slightly increases the current. As a result of the surface modification with the Fe_2O_3 clusters, the O_2 reduction current remarkably increases (Figure 7A). The O_2 reduction is also enhanced in the surface modification with Co_2O_3 (Figure

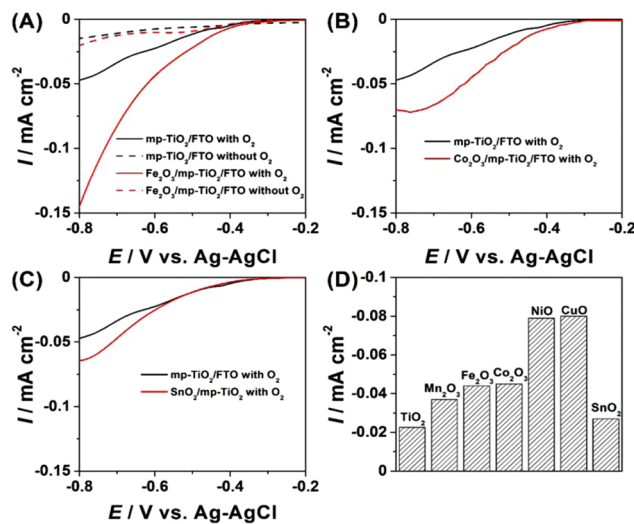


Figure 7. Current (I/mA)–potential (E/V vs Ag/AgCl) curves of the Fe_2O_3 /mp- TiO_2 (anatase)/FTO (A), Co_2O_3 /mp- TiO_2 /FTO (B), and SnO_2 /mp- TiO_2 /FTO (C) electrodes in a 0.1 M NaClO_4 aerated aqueous solution in the dark. (D) Dark currents at $E = -0.60 \text{ V}$ for MOs/ TiO_2 .

7B) and SnO_2 clusters (Figure 7C). A trend can be seen that the enhancing effect of O_2 reduction by the 3d MO cluster surface modification increases with increasing atomic number, whereas it is slight in the d¹⁰ SnO_2 cluster system (Figure 7D). Nosaka et al. suggested that the reduction of O_2 to H_2O_2 takes place in the Cu^{2+} -grafted TiO_2 system.²⁹ Also, the two-electron reduction has been achieved in the Rh^{3+} -grafted TiO_2 system, which can further enhance the O_2 reduction because it is thermodynamically more favorable ($E^0(\text{O}_2/\text{H}_2\text{O}_2) = +0.695 \text{ V}$) than the one-electron reduction.³⁰ The two-electron reduction may be responsible for the excellent O_2 reduction property of the CuO/TiO_2 system.

5. CATALYSIS

5.1. Thermocatalysis. 2-Naphthol, the starting material of azo dyes, was used as a model water pollutant. The thermocatalytic activity of $\text{Co}_2\text{O}_3/\text{TiO}_2$ for the degradation of 2-naphthol was examined at 323 K in the dark.²⁰ Figure 8A shows time courses for the 2-naphthol degradation at initial concentration of 2-naphthol ($[2\text{-naphthol}]_0 = 10 \mu\text{M}$) and catalyst concentration ([catalyst]) = 2 g L⁻¹. In the presence of unmodified TiO_2 and authentic Co_3O_4 (specific surface area = 4.4 m² g⁻¹), the 2-naphthol concentration is almost invariant. A

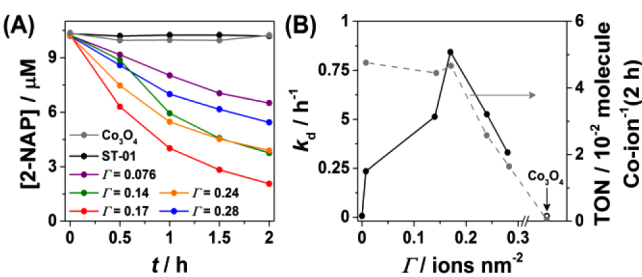


Figure 8. (A) Time courses for the $\text{Co}_2\text{O}_3/\text{TiO}_2$ (ST-01)-catalyzed 2-naphthol degradation in the dark at 323 K: initial concentration of 2-naphthol ($[2\text{-naphthol}]_0 = 10 \mu\text{M}$) and catalyst concentration ([catalyst]) = 2 g L⁻¹. (B) Plots of the rate constant vs Γ and TON vs Γ .

significant decrease in the 2-naphthol concentration is observed for the $\text{Co}_2\text{O}_3/\text{TiO}_2$ system. The turnover number (TON) reaches 8.6 at reaction time (t) = 22 h under the conditions of $[\text{2-naphthol}]_0 = 1 \text{ mM}$ and $[\text{Co}_2\text{O}_3(\Gamma = 0.17)/\text{TiO}_2] = 0.4 \text{ g L}^{-1}$. The rate of 2-naphthol degradation increased with increasing temperature with an activation energy of $46.5 \pm 0.4 \text{ kJ mol}^{-1}$. This thermocatalytic reaction apparently obeys the first-order rate law. Plots of the rate constant (k_d) vs Γ exhibit a volcano-shaped curve with a maximum k_d at $\Gamma \approx 0.17$ (Figure 8B). Clearly, the surface Co_2O_3 clusters act as catalytic active centers. 2-Naphthol was decomposed to CO_2 , and the amount increased almost in proportion to reaction time, although the decomposition was sluggish. As another test reaction, the degradation of formic acid was performed in the aqueous phase with $\text{Co}_2\text{O}_3/\text{TiO}_2$ at 323 K in the dark. While pristine TiO_2 shows a catalytic activity for the formic acid decomposition, it is remarkably accelerated by the surface modification of TiO_2 with Co_2O_3 clusters. At the optimum Γ of 0.17, the formic acid was completely decomposed to CO_2 at $t = 10 \text{ h}$.

Figure 9 compares the TONs at $t = 1 \text{ h}$ of 3d MOs/TiO₂ for the 2-naphthol degradation at 323 K. $\text{Mn}_2\text{O}_3/\text{TiO}_2$, $\text{Co}_2\text{O}_3/\text{TiO}_2$

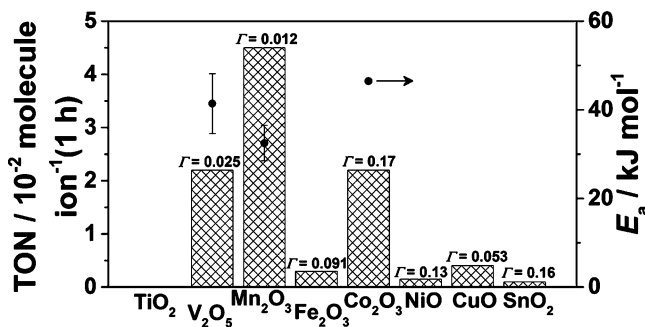


Figure 9. TONs at $t = 1 \text{ h}$ of MOs/TiO₂(ST-01) for the 2-naphthol degradation at 323 K and the activation energy (E_a). Each Γ was selected as the optimum value for visible-light activity (see Figure 12).

TiO_2 and $\text{V}_2\text{O}_5/\text{TiO}_2$ exhibit significant catalytic activity. The thermocatalytic activity is on the order of $\text{Mn}_2\text{O}_3 > \text{Co}_2\text{O}_3 \approx \text{V}_2\text{O}_5 \gg \text{CuO} > \text{Fe}_2\text{O}_3 > \text{NiO} \approx \text{SnO}_2 \approx \text{unmodified TiO}_2$, and the E_a values for Mn_2O_3 , Co_2O_3 , and V_2O_5 are comparable.

Bulk cobalt oxides containing Co ions in high oxidation states³¹ are known to have thermal catalytic activity for the decomposition of harmful organic compounds. Thermocatalytic activities far exceeding those of bulk Co_3O_4 and MnO_2 are imparted to TiO_2 by the surface modification of TiO_2 with Co_2O_3 ²⁰ and Mn_2O_3 clusters,³² respectively (fifth requirement). These results indicate that the high thermocatalytic activities can stem from the highly dispersed MO clusters on TiO_2 with a large surface area.

In the epoxidation of alkenes catalyzed by Co(III)-containing molecular sieves, Thomas and co-workers proposed an oxidation mechanism involving the electron transfer from benzaldehyde to Co³⁺ ions as the initiation step.³³ A similar redox mechanism was proposed in the present catalytic system.²⁰ The environments around the metal ions in the MOs/TiO₂ are close to those in hexa-aquo ions ($\text{M}^{n+}(\text{H}_2\text{O})_6$). Thus, the oxidizing power of the metal ion in the MO/TiO₂ would increase as the redox potential increases. Figure 10 shows plots of TONs versus standard redox potential of metal ions ($E^0(\text{M}^{n+}/\text{M}^{(n-1)+})$). The E^0 values for metal ions in the

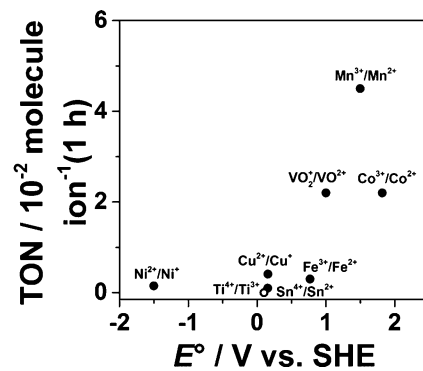


Figure 10. Plots of TONs at $t = 1 \text{ h}$ for MOs/TiO₂(ST-01) for the 2-naphthol degradation at 323 K vs $E^0(\text{M}^{n+}/\text{M}^{(n-1)+})$ for 3d MOs/TiO₂. Each Γ is the same as the value in Figure 9.

MOs/TiO₂ with catalytic activity are located at $E^0 > 1 \text{ V}$. This result suggests that the electron transfer from 2-naphthol to metal ions in the cluster is the key step.

5.2. Photocatalysis. Acetaldehyde, a volatile organic compound responsible for sick-house syndrome, was selected as a model air pollutant. Acetaldehyde as well as 2-naphthol are optically transparent in the visible region. The relative photocatalytic activities of various MOs/TiO₂ prepared by the CCC technique were assessed with respect to those of highly active anatase TiO_2 particles (ST-01) at 298 K. Under the conditions, the amounts of 2-naphthol (or acetaldehyde) adsorbed and thermocatalytically degraded were negligibly small as compared to those that are photocatalytically decomposed. The photocatalytic degradation of 2-naphthol and acetaldehyde apparently follow the first-order rate law, and the rate constants for irradiation of UV-light ($330 < \lambda < 400 \text{ nm}$, k_{UV}) and visible-light ($\lambda > 400 \text{ nm}$, k_{vis}) were employed as the indicators for the photocatalytic activities. Figure 11 shows

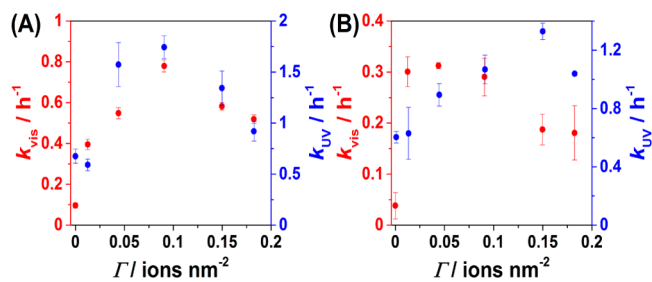


Figure 11. (A) UV-light activity (k_{UV} , blue) and visible-light activity (k_{vis} , red) of $\text{Fe}_2\text{O}_3/\text{TiO}_2$ (ST-01) for the liquid-phase decomposition of 2-NAP as a function of Γ . (B) UV-light activity (k_{UV} , blue) and visible-light activity (k_{vis} , red) of $\text{Fe}_2\text{O}_3/\text{TiO}_2$ (ST-01) for the gas-phase decomposition of CH_3CHO as a function of Γ .

the k_{vis} and k_{UV} of $\text{Fe}_2\text{O}_3/\text{TiO}_2$ for the degradations of 2-naphthol (A) and acetaldehyde (B) as a function of Γ . Surprisingly, the surface modification of TiO_2 with the Fe_2O_3 clusters causes a high level of visible-light activity and a concomitant increase in the UV-light activity of anatase TiO_2 . Each plot exhibits a volcano-shaped curve, which is a general feature in the plots for the MOs/TiO₂ systems. The Fe_2O_3 surface modification was effective also for P-25.¹⁶ By using an atomic layer deposition technique, Libera et al. prepared Fe(III)-oxo species surface-modified TiO_2 showing a reactivity

for the decoloration of methylene blue under visible-light irradiation.³⁴

Further, the degradation of formic acid was performed in the aqueous phase with $\text{Co}_2\text{O}_3/\text{TiO}_2$ (ST-01) at 298 K under visible-light irradiation. The Co_2O_3 surface modification greatly enhanced the decomposition of formic acid to CO_2 . The visible-light activity reached a maximum at $\Gamma = 0.17$, where the conversion to CO_2 reached $\sim 100\%$ within 5 h.²⁰ In general, particulate systems are highly active due to the large surface area, but the separation from purified water is troublesome, and supported films vice versa. The TiO_2 nanotube array having the advantages of the particulate and film systems is practically promising. The application of the CCC technique to the TiO_2 nanotube array gave rise to a high visible-light activity for 2-naphthol degradation comparable with that in a particulate system.¹⁹

Figure 12 compares the relative visible-light activity (k_{vis}) and UV-light activity (k_{UV}) of 3d MOs/ TiO_2 (ST-01) with respect

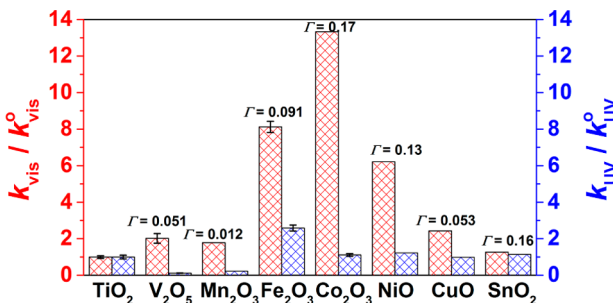
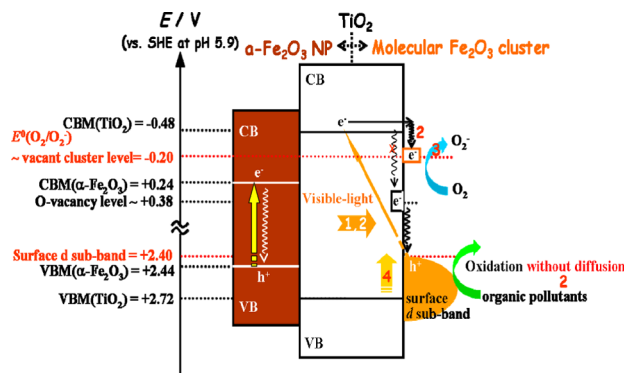


Figure 12. Comparison of the visible-light activities (k_{vis}) and UV-light activities (k_{UV}) of MOs/ TiO_2 (ST-01) for the 2-naphthol degradation under the same conditions.

to the activities of unmodified TiO_2 (k_{vis}^0 and k_{UV}^0) for 2-naphthol degradation under the same conditions. Each Γ is the optimum value for visible-light activity in each MO/ TiO_2 system. The surface modifications by the Fe_2O_3 ,¹⁶ Co_2O_3 ,²⁰ and NiO ³⁵ clusters are effective in visible-light activation. Among them, the $\text{Co}_2\text{O}_3/\text{TiO}_2$ system exhibits a very high level of visible-light activity, and fortunately, the optimum Γ value for the photocatalytic activity almost accords with that for its thermocatalytic activity. The activity is on the order of $\text{Co}_2\text{O}_3 > \text{Fe}_2\text{O}_3 > \text{NiO} > \text{CuO} > \text{V}_2\text{O}_5 \approx \text{Mn}_2\text{O}_3 > \text{SnO}_2 \approx \text{unmodified TiO}_2$. The UV-light activity increases with the surface modification by Fe_2O_3 clusters and is reduced for V_2O_5 and Mn_2O_3 clusters. The other Co_2O_3 , NiO , and CuO clusters hardly affect the UV-light activity. Obviously, the surface modification with Fe_2O_3 , NiO , and Co_2O_3 clusters by the CCC technique can endow anatase and anatase–rutile TiO_2 particles with high levels of visible-light activity, with the high UV-light activity further increased or maintained. Whereas the effect of the surface modification by SnO_2 clusters is small for anatase (Figure 12), a significant increase in the UV-light activity was induced for rutile.²⁵ Interestingly, Boppana and Lobo have recently reported that loading of SnO_x clusters on ZnGa_2O_4 by the impregnation method gives rise to visible-light activity for the decomposition of *p*-cresol.³⁶

On the basis of the energy band diagram for the MOs/ TiO_2 system, the action mechanism of MO nanocluster modified TiO_2 in photocatalysis can be explained. Scheme 2 compares the nanoscale (left side) and molecular scale (right side) Fe_2O_3 – TiO_2 heterojunction systems. In the nanocoupling

Scheme 2. Energy Band Diagrams of Fe_2O_3 – TiO_2 Coupling Systems: Nanoscale vs Molecular Scale



system, the band energy of each component is basically unmodified; similar considerations would hold for quantum dot³⁷ and molecular dye sensitized TiO_2 .³⁸ Upon visible-light irradiation, $\alpha\text{-Fe}_2\text{O}_3$ with a band gap of 2.2 eV is excited. The CB electrons, which lie too low in energy to transfer to the CB of TiO_2 , are destined to recombine with the VB holes because the CB minimum of $\alpha\text{-Fe}_2\text{O}_3$ (+0.24 V) is more positive than the reduction potential of O_2 ($E^0(\text{O}_2/\text{O}_2^-) = -0.20$ V). Consequently, the nanocoupling does not yield visible-light activity.³⁹ In QD or dye-sensitized TiO_2 , the CB of the absorber is higher in energy than the CB energy of TiO_2 , with transfer of the excited electron from the excited QD or dye to TiO_2 taking place. However, QD-sensitized TiO_2 suffers from, e.g., oxidation and rapid deactivation of the QD, which limits the practical application of this material system in photocatalysis.

On the other hand, in the molecular scale cluster– TiO_2 coupling system, the surface modification of TiO_2 by extremely small Fe_2O_3 clusters raises the VB maximum with the CB minimum unchanged, due to the effective electronic coupling through the new Fe–O–Ti interfacial bonds formed by the strong nanocluster– TiO_2 interaction (fourth requirement). The resulting decrease in the band gap shifts the light absorption to the visible region (first requirement). The visible-light absorption triggers electronic excitation from the highest-energy nanocluster derived VB states to the empty CB of TiO_2 , to generate charge carriers. This surface-to-bulk interfacial electron transfer (IET) enhances charge separation (second requirement). The surface modification can permit electron transfer from the CB(TiO_2) to shallow vacant surface nanocluster levels, for which the potential (-0.2 V) is close to the value for $E^0(\text{O}_2/\text{O}_2^-)$.⁴⁰ The formation of O_2^- radicals was confirmed by chemiluminescence photometry in the Cu^{2+} -grafted TiO_2 system under visible-light irradiation.²⁹ In the cathodic process, the electrons efficiently reduce adsorbed O_2 with the aid of the surface-adsorbed nanoclusters (third requirement). In the anodic process, the holes generated in the VB could take part in the oxidation process without diffusion.¹¹

5.3. Key Factors in the Surface Modification. First, the precise control for the amount of MO clusters on TiO_2 is important to realize high visible-light activity. Since the oxidation of 2-naphthol proceeds via the direct hole oxidation,⁶ an excess in the loading of the oxide nanoclusters will lower the oxidizing ability of the holes, as a consequence of the rise in the top of the VB, which reduces the activity. The resulting optimum loading amount of the modifying oxide nanocluster

depends on the nature of the modifying oxide nanocluster and the target pollutants. The ΔE_{VBM} values at the optimum Γ for the visible-light-induced 2-naphthol degradation in the $\text{Fe}_2\text{O}_3/\text{TiO}_2$ and $\text{Co}_2\text{O}_3/\text{TiO}_2$ systems are comparable (~ 0.4 eV). Also, in the $\text{Fe}_2\text{O}_3/\text{TiO}_2$ system, the optimum Γ for the acetaldehyde degradation (~ 0.1) is smaller than that for the 2-naphthol degradation (~ 0.5). This is probably because acetaldehyde ($E_{\text{HOMO}} = -6.72$ eV vs vacuum) is harder to be oxidized than 2-naphthol ($E_{\text{HOMO}} = -5.57$ eV vs vacuum).⁶ Further, it is worthy noting that the decomposition of model organic pollutants to CO_2 proceeds in the $\text{Co}_2\text{O}_3/\text{TiO}_2$ system despite that the ΔE_{VBM} is large. The DFT simulations for this system suggest that the strong oxidation ability could arise from the VB holes of TiO_2 generated by the visible-light-induced IET from the VB of TiO_2 to the vacant surface Co_2O_3 cluster levels (bulk-to-surface IET) concomitantly with the surface-to-bulk IET.

Second, as suggested by the DFT simulations, the cluster size affects the catalytic activities of MOs/TiO₂. The TON of $\text{Co}_2\text{O}_3/\text{TiO}_2$ -thermocatalyzed degradation of 2-naphthol at 2 h is almost constant at $\Gamma < 0.17$, steeply decreasing at $\Gamma > 0.17$ (Figure 8B). The TEM observation and UV-visible absorption spectra indicate that the Co_2O_3 cluster size is a factor governing the thermocatalytic activity. Also, the appearance of the d-d transition with the growth of MO clusters generally decreases the visible-light activity. In a single crystal of $[\text{Ru}(\text{bpy})_3](\text{PF}_6)_2$, the d-d transition is known to shorten the lifetime of the charge-transfer excited state.⁴¹ This may also be valid for the MOs/TiO₂ system because the excitation energies of the charge-transfer and the d-d transition are comparable.

Third, the surface modification effect on the TiO₂ activity can depend on not only the kind of MOs but also its crystal form. Grafting of Fe³⁺ ions onto rutile gives rise to a high level of visible-light activity; however, it is minor for anatase.¹⁴ Also, the surface modification of rutile TiO₂ with SnO₂ clusters leads to an increase in its UV-light activity, whereas it is ineffective for anatase.³⁵ The DFT simulations for model structures show that although SnO₂ nanoclusters are strongly adsorbed onto surfaces of both TiO₂ crystal forms the interface structure and electronic density of states present significant differences between rutile and anatase. For rutile, the changed DOS due to SnO₂ states at the CB increases light absorption and enhances charge separation. In contrast, for anatase, SnO₂ states lie above the TiO₂ CB. On the other hand, for other transition metal oxide-modified TiO₂, the crystal form of TiO₂ has little effect. In this manner, the DFT simulation-assisted rational design is very effective in the development of the metal oxide surface-modified TiO₂.

6. CONCLUSIONS AND FUTURE PROSPECT

Molecular-scale oxides of 3d metals and d¹⁰ metal (SnO₂) can be formed on TiO₂ with the loading amount precisely controlled by using the CCC technique. We have presented the guideline for increasing the thermocatalytic and photocatalytic activity of MOs/TiO₂ for the oxidative degradations of organic pollutants. In view of thermocatalysis of MOs/TiO₂, the redox potential of metal ions in aqueous solution can be a useful parameter; i.e., the activity tends to increase as the value becomes more positive. Among 3d MOs/TiO₂, Mn₂O₃/TiO₂, Co₂O₃/TiO₂, and V₂O₅/TiO₂ exhibit significant thermocatalytic activity. Unlike SnO₂/TiO₂, some 3d MO cluster surface-modified TiO₂ possesses unique physicochemical properties such as strong visible-light absorption and excellent reduction

ability of O₂. Spectroscopic experiments and first-principles DFT simulation have revealed that the surface modification with the MO clusters raises the VB maximum of TiO₂ due to the formation of plural metal–O–Ti interfacial bonds. Surface-to-bulk (and bulk-to-surface for the Co₂O₃/TiO₂ system) IET accompanied by visible-light absorption enhance charge separation. Particularly, in the Co₂O₃/TiO₂ system, the compatibility of high levels of photocatalytic and thermocatalytic activities is achieved. This new coupling system consisting of molecular-scale MOs and TiO₂ would be promising as a solar environmental catalyst for purifying water and air efficiently using solar energy. Further, the fine-tuning of the VB-maximum level by the loading amount of MO clusters would open up the application of MOs/TiO₂ to “green” and selective chemical transformations.^{42,43}

■ AUTHOR INFORMATION

Corresponding Author

*E-mail: h-tada@apch.kindai.ac.jp.

Notes

The authors declare no competing financial interest.

Biographies



Hiroaki Tada received his BSc and MSc in Engineering from Kyoto University. He received his Dr. degree in Engineering from Kyoto University in 1991. He joined the research group of Prof. A. T. Bell at University of California, Berkeley as an invited scholar in 2002. He has been a full professor of School of Science and Engineering at Kinki University since 2005.



Liliang Jin was born in China. He obtained a BSc and MSc in Engineering from Kinki University in 2009 and 2011. He completed his PhD studies on surface modified TiO₂ under the tuition of Prof. Tada at Kinki University in 2014.



Anna Iwaszuk was born in Poland. She obtained a BSc in Analytical Chemistry from Hogeschool Zeeland in The Netherlands and MSc in Chemical and Process Engineering from Technical University of Szczecin, Poland. She completed her PhD studies on surface modified TiO₂ with Dr. Nolan at the Tyndall National Institute in 2013 and now works with Pfizer Pharmaceuticals.



Michael Nolan received a BSc in Chemistry with German in 1997 and a Masters and PhD in Microelectronic Engineering from University College Cork in 1999 and 2004. He was a postdoctoral fellow at Trinity College Dublin with Prof. Graeme Watson and has been at Tyndall National Institute since 2005 and a staff researcher since 2009.

ACKNOWLEDGMENTS

The authors acknowledge Dr. M. Fujishima (Kinki University) for valuable discussion and T. Hattori, S. Okuoka, and Y. Sumida (Nippon Shokubai Co.) for EXAFS measurements and valuable discussion. Ishihara Sangyo Co. gifted us with ST-01. H.T. acknowledges support from the Ministry of Education, Science, Sport, and Culture, Japan through a Grant-in-Aid for Scientific Research (C) No. 24550239, and Nippon Sheet Glass Foundation for Materials Science and Engineering, and by Sumitomo Foundation. M.N. acknowledges support from Science Foundation Ireland through the Starting Investigator Research Grant Program, project "EMOIN" grant number SFI 09/SIRG/I1620. We also acknowledge computing resources provided by SFI to the Tyndall National Institute and by the SFI and Higher Education Authority Funded Irish Centre for High End Computing. Support from the European Commission for access through the FP7 Research Infrastructures Project PRACE-RI is gratefully acknowledged. We acknowledge support from the European Union through the COST Action CM1104 "Reducible Oxide Chemistry, Structure and Functions".

REFERENCES

- (1) Hashimoto, K.; Irie, H.; Fujishima, A. TiO₂ Photocatalysis: A Historical Overview and Future Prospects. *Jpn. J. Appl. Phys.* **2005**, *44*, 8269–8285.
- (2) Park, H.; Park, Y.; Kim, W.; Choi, W. Surface Modification of TiO₂ Photocatalyst for Environmental Applications. *J. Photochem. Photobiol. C* **2013**, *15*, 1–20.
- (3) Zhang, H.; Chen, G.; Bahnemann, D. W. Photoelectrocatalytic Materials for Environmental Applications. *J. Mater. Chem.* **2009**, *19*, 5089–5121.
- (4) Liu, G.; Wang, L.; Yang, H. G.; Cheng, H.-M.; Lu, G. Q. Titania-Based Photocatalysts-Crystal Growth, Doping and Heterostructuring. *J. Mater. Chem.* **2010**, *20*, 831–843.
- (5) Henderson, M. A. A Surface Science Perspective on TiO₂ Photocatalysis. *Surf. Sci. Rep.* **2011**, *66*, 185–297.
- (6) Tada, H.; Jin, Q.; Kobayashi, H. Prediction of the Main Route in the TiO₂-Photocatalyzed Degradation of Organic Compounds in Water by Density Functional Calculations. *ChemPhysChem* **2012**, *13*, 3457–3461.
- (7) Prieto-Mahaney, O.-O.; Murakami, N.; Abe, R.; Ohtani, B. Correlation Between Photocatalytic Activities and Structural and Physical Properties of Titanium(IV) Oxide Powders. *Chem. Lett.* **2009**, *38*, 238–239.
- (8) Ahmed, A. Y.; Kandiel, T. A.; Oekermann, T.; Bahnemann, D. W. Photocatalytic Activities of Different Well-defined Single Crystal TiO₂ Surfaces: Anatase versus Rutile. *J. Phys. Chem. Lett.* **2011**, *2*, 2461–2465.
- (9) Kawahara, T.; Konishi, Y.; Tada, T.; Tohge, N.; Nishii, J.; Ito, S. A Patterned TiO₂(Anatase)/TiO₂(Rutile) Bilayer-Type Photocatalyst: Effect of the Anatase/Rutile Junction on the Photocatalytic Activity. *Angew. Chem., Int. Ed.* **2002**, *41*, 2811–2813.
- (10) Kisch, H. Semiconductor Photocatalysis-Mechanistic and Synthetic Aspects. *Angew. Chem., Int. Ed.* **2013**, *52*, 812–847.
- (11) Irie, H.; Shibanuma, T.; Kamiya, K.; Miura, S.; Yokoyama, T.; Hashimoto, K. Characterization of Cr(III)-Grafted TiO₂ for Photocatalytic Reaction Under Visible Light. *Appl. Catal., B* **2010**, *96*, 142–147.
- (12) Yu, H.; Irie, H.; Hashimoto, K. Conduction Band Energy Level Control of Titanium Dioxide: Toward an Efficient Visible-Light-Sensitive Photocatalyst. *J. Am. Chem. Soc.* **2010**, *132*, 6898–6899.
- (13) Murakami, N.; Chiyo, T.; Tsubota, T.; Ohno, T. Switching Redox Site of Photocatalytic Reaction on Titanium(IV) Oxide Particles Modified with Transition-Metal Ion Controlled by Irradiation Wavelength. *Appl. Catal., A* **2008**, *348*, 148–152.
- (14) Yu, H.; Irie, H.; Shimodaira, Y.; Hosogi, Y.; Kuroda, Y.; Miyauchi, M.; Hashimoto, K. An Efficient Visible-Light-Sensitive Fe(III)-Grafted TiO₂ Photocatalyst. *J. Phys. Chem. C* **2010**, *114*, 16481–16487.
- (15) Tada, H. *Encyclopedia of Surface and Colloid Science*; Hubbard, A. T., Ed.; Marcel Dekker: New York, 2002.
- (16) Tada, H.; Jin, Q.; Nishijima, H.; Yamamoto, H.; Fujishima, M.; Okuoka, S.-i.; Hattori, T.; Sumida, Y.; Kobayashi, H. Titanium(IV) Dioxide Surface-Modified with Iron Oxide as a Visible Light Photocatalyst. *Angew. Chem., Int. Ed.* **2011**, *50*, 3501–3505.
- (17) Jin, Q.; Fujishima, M.; Iwaszuk, A.; Nolan, M.; Tada, H. Loading Effect in Copper(II) Oxide Cluster-Surface-Modified Titanium(IV) Oxide on Visible- and UV-Light Activities. *J. Phys. Chem. C* **2013**, *117*, 23848–23857.
- (18) Fujishima, M.; Jin, Q.; Yamamoto, H.; Tada, H.; Nolan, M. Tin Oxide-Surface Modified Anatase Titanium(IV) Dioxide with Enhanced UV-Light Photocatalytic Activity. *Phys. Chem. Chem. Phys.* **2012**, *14*, 705–711.
- (19) Muramatsu, Y.; Jin, Q.; Fujishima, M.; Tada, H. Visible-Light-Activation of TiO₂ Nanotube Array by The Molecular Iron Oxide Surface Modification. *Appl. Catal. B: Environ.* **2012**, *119–120*, 74–80.
- (20) Jin, Q.; Yamamoto, H.; Yamamoto, K.; Fujishima, M.; Tada, H. Simultaneous Induction of High Level Thermal and Visible-Light Catalytic Activities to Titanium(IV) Oxide by Surface Modification

- with Cobalt(III) Oxide Clusters. *Phys. Chem. Chem. Phys.* **2013**, *15*, 20313–20319.
- (21) Iwaszuk, A.; Mulheran, P. A.; Nolan, M. TiO₂ Nanocluster Modified-Rutile TiO₂ Photocatalyst: A First Principles Investigation. *J. Mater. Chem. A* **2013**, *1*, 2515–2525.
- (22) Nolan, M. Electronic Coupling in Iron Oxide-Modified TiO₂ Leads to a Reduced Band Gap and Charge Separation for Visible Light Active Photocatalysis. *Phys. Chem. Chem. Phys.* **2011**, *13*, 18194–18199.
- (23) Iwaszuk, A.; Nolan, M. SnO-Nanocluster Modified Anatase TiO₂ Photocatalyst: Exploiting the Sn(II) Lone Pair for a New Photocatalyst Material with Visible Light Absorption and Charge Carrier Separation. *J. Mater. Chem. A* **2013**, *1*, 6670–6677.
- (24) Anpo, M.; Takeuchi, M. The Design and Development of Highly Reactive Titanium Oxide Photocatalysts Operating Under Visible Light Irradiation. *J. Catal.* **2003**, *216*, 505–516.
- (25) Jin, Q.; Fujishima, M.; Nolan, M.; Iwaszuk, A.; Tada, H. Photocatalytic Activities of Tin(IV) Oxide Surface-Modified Titanium(IV) Dioxide Show a Strong Sensitivity to the TiO₂ Crystal Form. *J. Phys. Chem. C* **2012**, *116*, 12621–12626.
- (26) Iwaszuk, A.; Nolan, M. Lead Oxide-Modified TiO₂ Photocatalyst: Tuning Light Absorption and Charge Carrier Separation by Lead Oxidation State. *Catal. Sci. Technol.* **2013**, *3*, 2000–2008.
- (27) Nolan, M. Surface Modification of TiO₂ with Metal Oxide Nanoclusters: A Route to Composite Photocatalytic Materials. *Chem. Commun.* **2011**, *47*, 8617–8619.
- (28) Wang, C. M.; Heller, A.; Gerischer, H. Palladium Catalysis of O₂ Reduction by Electrons Accumulated on TiO₂ Particles During Photoassisted Oxidation of Organic Compounds. *J. Am. Chem. Soc.* **1992**, *114*, 5230–5234.
- (29) Nosaka, Y.; Takahashi, S.; Sakamoto, H.; Nosaka, A. Y. Reaction Mechanism of Cu(II)-Grafted Visible-Light Responsive TiO₂ and WO₃ Photocatalysts Studied by Means of ESR Spectroscopy and Chemiluminescence Photometry. *J. Phys. Chem. C* **2011**, *115*, 21283–21290.
- (30) Kitano, S.; Murakami, N.; Ohno, T.; Mitani, Y.; Nosaka, Y.; Asakura, H.; Teramura, K.; Tanaka, T.; Tada, H.; Hashimoto, K.; et al. Bifunctionality of Rh³⁺ Modifier on TiO₂ and Working Mechanism of Rh³⁺/TiO₂ Photocatalyst Under Irradiation of Visible Light. *J. Phys. Chem. C* **2013**, *117*, 11008–11016.
- (31) Martyanov, I. N.; Umas, S.; Rodrigues, S.; Klabunde, K. J. Decontamination of Gaseous Acetaldehyde Over CoO_x-Loaded SiO₂ Xerogels Under Ambient, Dark Conditions. *Langmuir* **2005**, *21*, 2273–2280.
- (32) Jin, Q.; Arimoto, H.; Fujishima, M.; Tada, H. Manganese Oxide-Surface Modified Titanium(IV) Dioxide as Environmental Catalyst. *Catalysts* **2013**, *3*, 444–454.
- (33) Raja, R.; Sankar, G.; Thomas, J. M. New Catalysts for The Aerobic Selective Oxidation of Hydrocarbons: Mn(III)- and Co(III)-Containing Molecular Sieves for The Epoxidation of Alkenes. *Chem. Commun.* **1999**, 829–830.
- (34) Libera, J. A.; Elam, J. W.; Sather, N. F.; Rajh, T.; Dimitrijevic, N. M. Iron(III)-oxo Centers on TiO₂ for Visible-Light Photocatalysis. *Chem. Mater.* **2010**, *22*, 409–413.
- (35) Jin, Q.; Ikeda, T.; Fujishima, M.; Tada, H. Nickel(II) Oxide Surface-Modified Titanium(IV) Dioxide as a Visible-Light-Active Photocatalyst. *Chem. Commun.* **2011**, *47*, 8814–8816.
- (36) Boppana, V. B. R.; Lobo, R. F. SnO_x-ZnGa₂O₄ Photocatalysts with Enhanced Visible Light Activity. *ACS Catal.* **2011**, *1*, 923–928.
- (37) Tada, H.; Fujishima, M.; Kobayashi, H. Photodeposition of Metal Sulfide Quantum Dots on Titanium(IV) Dioxide and the Applications to Solar Energy Conversion. *Chem. Soc. Rev.* **2011**, *40*, 4232–4243.
- (38) Grätzel, M. Photoelectrochemical Cells. *Nature* **2001**, *414*, 338–344.
- (39) Lin, X.; Li, D.-Z.; Wu, Q.-P.; Fu, X.-Z.; Wang, X.-X. Photocatalytic Activity and Mechanism of Heterojunction Thin Films. *Chem. J. Chin. Univ.* **2005**, *26*, 727–730.
- (40) Jin, Q.; Fujishima, M.; Tada, H. Visible-Light-Active Iron Oxide-Modified Anatase Titanium(IV) Dioxide. *J. Phys. Chem. C* **2011**, *115*, 6478–6483.
- (41) Islam, A.; Ikeda, N.; Nozaki, K.; Ohno, T. Role of Higher Excited States in Radiative and Nonradiative Processes of Coordination Compounds of Ru(II) and Rh(III) in Crystal. *Chem. Phys. Lett.* **1996**, *263*, 209–214.
- (42) Ide, Y.; Hattori, H.; Ogo, S.; Sadakane, M.; Sano, T. Highly Efficient and Selective Sunlight-Induced Photocatalytic Oxidation of Cyclohexane on An Eco-Catalyst Under a CO₂ Atmosphere. *Green Chem.* **2012**, *14*, 1264–1267.
- (43) Higashimoto, S.; Shirai, R.; Osano, Y.; Azuma, M.; Ohue, H.; Sakata, Y.; Kobayashi, H. Influence of Metal Ions on the Photocatalytic Activity: Selective Oxidation of Benzyl Alcohol on Iron(III) Ion-Modified TiO₂ Using Visible Light. *J. Catal.* **2014**, *311*, 137–143.